Noname manuscript No.
(will be inserted by the editor)

N.M.A.Nik Long · R.A.Rafar · N.Senu · N.A.Noda

Stress intensity factor for multiple inclined or curved cracks problem in circular positions in plane elasticity

Received: date / Accepted: date

Abstract The problems of an infinite plate containing multiple inclined or curved cracks in circular positions is treated by using the hypersingular integral equation method. The cracks center are placed at the edge of a virtual circle with radius R. The first crack is fixed on the x-axis while the second crack is located on the boundary of a circle with the varying angle, θ. A system of hypersingular integral equations is formulated and solved numerically for the unknown coefficients. The obtained unknown coefficients are then used for determining the stress intensity factor (SIF). Numerical examples demonstrate the effect of interaction between two cracks in circular positions are given. It is found that, the severity at the second crack tips are significant when the ratio length of the second to the first crack is small and it is placed at a small angle of θ.

Keywords Stress Intensity Factor · Multiple Inclined or Curved Cracks · Circular Position · Hypersingular Integral Equation

1 Introduction

The multiple cracks problems that involved arbitrarily crack arrangement are common in many engineering structures. The multiple two dimensional problems of inclined and curved cracks can be investigated by determining the stress intensity factor (SIF). In previous years, Vialaton et al. [7] used the complex potential method to determine the SIF for two identical length of collinear cracks in an infinite plate under arbitrary concentrated loading. Kachanov [9,10] showed that the interaction of multiple cracks problems can be solved with the help of a superposition technique which leads to a system of linear algebraic equations. Furthermore, many researchers used the integral equation methods for the numerical solution of multiple cracks problems. For example, Panasyuk et al. [8] presented

N. M. A. Nik Long
Mathematics Department, Faculty of Science, Universiti Putra Malaysia, 43400 Serdang, Selangor, Malaysia
Institute for Mathematical Research, Universiti Putra Malaysia, Serdang, Selangor, Malaysia
Tel.: +603-8946 6811
Fax: +603-8943 7958
E-mail: nmasri@upm.edu.my

R. A. Rafar
Mathematics Department, Faculty of Science, Universiti Putra Malaysia, 43400 Serdang, Selangor, Malaysia
E-mail: eimah7178@gmail.com

N. Senu
Institute for Mathematical Research, Universiti Putra Malaysia, Serdang, Selangor, Malaysia
Mathematics Department, Faculty of Science, Universiti Putra Malaysia, 43400 Serdang, Selangor, Malaysia

N. A. Noda
Kyushu Institute of Technology, Kitakyushu, Japan
E-mail: noda@mech.kyutech.ac.jp

a singular integral equation using a perturbation method to solve multiple cracks problems. Chen [11] used the complex variable function method to formulate the singular integral equation for multiple curved cracks problems. In addition, Chen and Lin [12] investigated the multiple curved branch-cracks in term of singular integral equation. Helsing [13] proposed a scheme for the numerical solution of singular integral equations on piecewise smooth curves. Chen [16] and Chen et al. [2] used the Fredholm integral equation to solve multiple cracks problems. Hypersingular integral equation has also been used to solve the multiple cracks problems. For example, Chen [17] solved the hypersingular integral equation in a closed form which the unknowns are approximated by a weight function multiplied by a polynomial. In addition, Nik Long and Eshkuvatov [3], Aridi et al. [19] and Nik Long et al. [5] used the complex variable function method to formulate the hypersingular integral equation. The curved length coordinate method is then used to solve the hypersingular integral equation numerically. Zozulya [20] developed hypersingular integral regularization and applied it for the case of three dimensional crack problem. Moreover, Wang et al. [21] used hypersingular integral equation to formulate and solve the micromechanical models.

Formulation in terms of hypersingular integral equation for solving the problem of multiple inclined or curved cracks in circular positions in plane elasticity is studied in this paper. Numerical examples are given to show the behavior of the SIF at the crack tips, and are presented and displayed graphically.

2 Complex variable function method

The stresses $(\sigma_x, \sigma_y, \sigma_{xy})$, the resultant force functions (X, Y) and the displacements (u, v) are related to the complex potentials $\Phi(z)$ and $\Psi(z)$ as follows [1]

$$\sigma_x + \sigma_y = 4Re\Phi(z), \tag{1}$$

$$\sigma_y - \sigma_x + 2i\sigma_{xy} = 2[\bar{z}\Phi'(z) + \Psi(z)], \tag{2}$$

$$f = -Y + iX = \phi(z) + z\overline{\phi'(z)} + \overline{\psi(z)} + c, \tag{3}$$

$$2G(u + iv) = K\phi(z) - z\overline{\phi'(z)} + \psi(z), \tag{4}$$

where $\Phi(z) = \phi'(z)$ and $\Psi(z) = \psi'(z)$, G is shear modulus of elasticity, $K = (3 - v)/(1 + v)$ for plane stress, $K = 3 - v$ for plane strain, v as Poisson's ratio, and $z = x + iy$. The derivative in a specified direction (abbreviated as DISD) is defined as follows

$$\frac{d}{dz}\{-Y + iX\} = \Phi(z) + \overline{\Phi(z)} + \frac{d\bar{z}}{dz}\left(z\overline{\Phi'(z)} + \overline{\Psi(z)}\right) = N + iT, \tag{5}$$

where $N + iT$ denotes the tractions along the segment $\overline{z, z + dz}$. The value of $N + iT$ depends on both the position of point z as well as on the direction of the segment $d\bar{z}/dz$ [2,3].

By placing two point dislocations with intensity $H(-H)$ at point $z = t(z = t + dt)$, the complex potentials $\phi(z)$ and $\psi(z)$ are obtained as follows

$$\begin{aligned} \phi(z) &= -H\frac{dt}{z - t}, \\ \psi(z) &= -\overline{H}\frac{dt}{z - t} - H\frac{d\bar{t}}{t - z} + H\frac{\bar{t}dt}{(t - z)^2}. \end{aligned} \tag{6}$$

Next, the new form of complex potential functions are obtained by substituting $H(\overline{H})$ with $-g(t)/2\pi(-\overline{g(t)}/2\pi)$ in Eq. (6) and integrate along the crack configuration, yield

$$\begin{aligned} \phi(z) &= \frac{1}{2\pi}\int_L \frac{g(t)dt}{t - z}, \\ \psi(z) &= \frac{1}{2\pi}\int_L \frac{g(t)d\bar{t}}{t - z} + \frac{1}{2\pi}\int_L \frac{\overline{g(t)}dt}{t - z} - \frac{1}{2\pi}\int_L \frac{\bar{t}g(t)dt}{(t - z)^2}. \end{aligned} \tag{7}$$

Substituting Eq. (7) into Eq. (4), and by letting the moving point z approaches t_0^+ and t_0^-, which are located on the upper and lower sides of the crack faces (Fig. 1), then using the generalized Plemelj equation, and rewritting t_0 as t, we get [2,3]

$$2G(u(t)+iv(t)) = i(k+1)g(t), \quad t \in L, \tag{8}$$

where $(u(t)+iv(t)) = (u(t)+iv(t))^+ - (u(t)+iv(t)^-$ is the crack opening displacement (COD) for the straight cracks. It is well known that the COD possesses the following properties

$$\begin{aligned} g(t) &= O[\sqrt{t-t_{A_j}}] \text{ at the crack tip } A_j, \ j=1,2, \\ g(t) &= O[\sqrt{t-t_{B_j}}] \text{ at the crack tip } B_j. \ j=1,2. \end{aligned} \tag{9}$$

3 Hypersingular integral equations

Hypersingular integral equation for single inclined and single curved crack problem is given by [2]

$$\frac{1}{\pi}\oint\!\!\!\!\!\!-_L \frac{g(t)dt}{(t-t_0)^2} + \frac{1}{2\pi}\int_L K_1(t,t_0)g(t)dt + \frac{1}{2\pi}\int_L K_2(t,t_0)\overline{g(t)}dt = N(t_0)+iT(t_0), \quad t_0 \in L, \tag{10}$$

where

$$\begin{aligned} K_1(t,t_0) &= -\frac{1}{(t-t_0)^2} + \frac{1}{(\bar{t}-\bar{t}_0)^2}\frac{d\bar{t}_0}{dt_0}\frac{d\bar{t}}{dt} \\ K_2(t,t_0) &= -\frac{1}{(\bar{t}-\bar{t}_0)^2}\left(\frac{d\bar{t}}{dt}+\frac{d\bar{t}_0}{dt_0}\right) - \frac{2(t-t_0)}{(\bar{t}-\bar{t}_0)^3}\frac{d\bar{t}_0}{dt_0}\frac{d\bar{t}}{dt} \end{aligned}$$

and $g(t)$ is the dislocation distribution along the crack. In Eq. (10), the first integral with equal sign on it denotes the hypersingular integral and should be defined in the sense of Hadamart finite part integral.

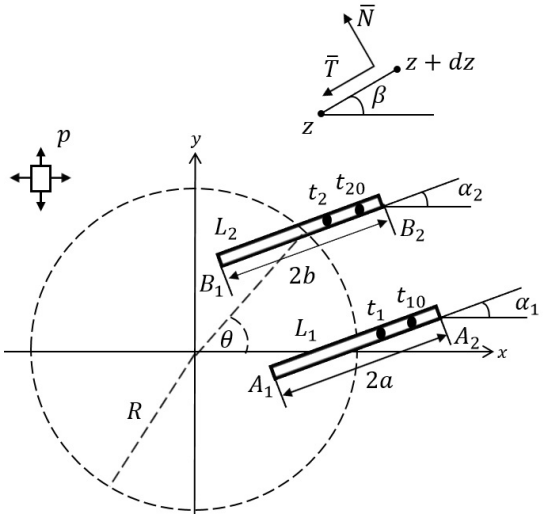

Fig. 1 Two inclined cracks placed in a circular position in plane elasticity.

Consider the interaction between two inclined cracks problem (Fig. 1). Two inclined cracks are subjected to the remote tension $\sigma_x^\infty = \sigma_y^\infty = p$. Applying superposition of the dislocation doublet

distribution $g_1(t_1)$ along L_1 and the dislocation doublet distribution $g_2(t_2)$ along L_2, we obtain the hypersingular integral equation for L_1 which is

$$\frac{1}{\pi}\oint\!\!\!\!\!\!=_{L_1}\frac{g_1(t_1)dt_1}{(t_1-t_{10})^2}+\frac{1}{2\pi}\int_{L_1}K_1(t_1,t_{10})g_1(t_1)dt_1+\frac{1}{2\pi}\int_{L_1}K_2(t_1,t_{10})\overline{g_1(t_1)}dt_1+\frac{1}{\pi}\int_{L_2}\frac{g_2(t_2)dt_2}{(t_2-t_{10})^2}$$
$$+\frac{1}{2\pi}\int_{L_2}K_1(t_2,t_{10})g_2(t_2)dt_2+\frac{1}{2\pi}\int_{L_2}K_2(t_2,t_{10})\overline{g_2(t_2)}dt_2=N_1(t_{10})+iT_1(t_{10}) \tag{11}$$

where $N_1(t_{10})+iT_1(t_{10})$ is the traction applied at point t_{10} of L_1, which is derived from the boundary condition and

$$K_1(t_1,t_{10})=-\frac{1}{(t_1-t_{10})^2}+\frac{1}{(\bar{t}_1-\bar{t}_{10})^2}\frac{d\bar{t}_{10}}{dt_{10}}\frac{d\bar{t}_1}{dt_1},$$
$$K_2(t_1,t_{10})=-\frac{1}{(\bar{t}_1-\bar{t}_{10})^2}\left(\frac{d\bar{t}_1}{dt}+\frac{d\bar{t}_{10}}{dt_{10}}\right)-\frac{2(t_1-t_{10})}{(\bar{t}_1-\bar{t}_{10})^3}\frac{d\bar{t}_{10}}{dt_{10}}\frac{d\bar{t}_1}{dt_1},$$
$$K_1(t_2,t_{10})=-\frac{1}{(t_2-t_{10})^2}+\frac{1}{(\bar{t}_2-\bar{t}_{10})^2}\frac{d\bar{t}_{10}}{dt_{10}}\frac{d\bar{t}_2}{dt_2},$$
$$K_2(t_2,t_{10})=-\frac{1}{(\bar{t}_2-\bar{t}_{10})^2}\left(\frac{d\bar{t}_2}{dt_2}+\frac{d\bar{t}_{10}}{dt_{10}}\right)-\frac{2(t_2-t_{10})}{(\bar{t}_2-\bar{t}_{10})^3}\frac{d\bar{t}_{10}}{dt_{10}}\frac{d\bar{t}_2}{dt_2}.$$

Similarly, the hypersingular integral equation for L_2 is

$$\frac{1}{\pi}\oint\!\!\!\!\!\!=_{L_2}\frac{g_2(t_2)dt_2}{(t_2-t_{20})^2}+\frac{1}{2\pi}\int_{L_2}K_1(t_2,t_{20})g_2(t_2)dt_2+\frac{1}{2\pi}\int_{L_2}K_2(t_2,t_{20})\overline{g_2(t_2)}dt_2+\frac{1}{\pi}\int_{L_1}\frac{g_1(t_1)dt_1}{(t_1-t_{20})^2}$$
$$+\frac{1}{2\pi}\int_{L_1}K_1(t_1,t_{20})g_1(t_1)dt_1+\frac{1}{2\pi}\int_{L_1}K_2(t_1,t_{20})\overline{g_1(t_1)}dt_1=N_2(t_{20})+iT_2(t_{20}) \tag{12}$$

where $N_2(t_{20})+iT_2(t_{20})$ is the traction applied at point t_{20} of L_2 and

$$K_1(t_2,t_{20})=-\frac{1}{(t_2-t_{20})^2}+\frac{1}{(\bar{t}_2-\bar{t}_{20})^2}\frac{d\bar{t}_{20}}{dt_{20}}\frac{d\bar{t}_2}{dt_2},$$
$$K_2(t_2,t_{20})=-\frac{1}{(\bar{t}_2-\bar{t}_{20})^2}\left(\frac{d\bar{t}_2}{dt_2}+\frac{d\bar{t}_{20}}{dt_{20}}\right)-\frac{2(t_2-t_{20})}{(\bar{t}_2-\bar{t}_{20})^3}\frac{d\bar{t}_{20}}{dt_{20}}\frac{d\bar{t}_2}{dt_2},$$
$$K_1(t_1,t_{20})=-\frac{1}{(t_1-t_{20})^2}+\frac{1}{(\bar{t}_1-\bar{t}_{20})^2}\frac{d\bar{t}_{20}}{dt_{20}}\frac{d\bar{t}_1}{dt_1},$$
$$K_2(t_1,t_{20})=-\frac{1}{(\bar{t}_1-\bar{t}_{20})^2}\left(\frac{d\bar{t}_1}{dt_1}+\frac{d\bar{t}_{20}}{dt_{20}}\right)-\frac{2(t_1-t_{20})}{(\bar{t}_1-\bar{t}_{20})^3}\frac{d\bar{t}_{20}}{dt_{20}}\frac{d\bar{t}_1}{dt_1}.$$

Equations (11) and (12) are solved for $g_1(t_1)$ and $g_2(t_2)$ concurrently.

4 Numerical Examples

Two inclined cracks configurations are projected onto a real axis with interval of $2a$ and $2b$ by using the mapping functions $t_1(s_1)$ and $t_2(s_2)$, respectively. The functions $g_1(t_1)$ and $g_2(t_2)$ can be defined as follows

$$g_1(t_1)|_{t_1=t_1(s_1)}=\sqrt{a^2-s_1^2}H_1(s_1), \tag{13}$$
$$g_2(t_2)|_{t_2=t_2(s_2)}=\sqrt{b^2-s_2^2}H_2(s_2), \tag{14}$$

where $H_1(s_1)=H_{11}(s_1)+iH_{12}(s_1)$ and $H_2(s_2)=H_{21}(s_2)+iH_{22}(s_2)$. Using these conversions, the system of integral equations in (11) and (12) can be evaluate numerically. Consider the following examples.

4.1 Example 1

Consider the interaction between two inclined cracks in circular positions in an infinite plate. For comparison purposes, two inclined cracks are under uniaxial tension $\sigma_y^\infty = p$ (Fig. 2). Both cracks are placed on the boundary of the virtual circle where the second crack, L_2, lies at an angle $\theta = 180°$. The calculated results for the SIFs at the crack tips A_1, A_2, B_1, and B_2 are expressed as

$$\begin{aligned} K_{1A_1} &= K_{1B_2} = F_{1B_2}(2a/d)p\sqrt{\pi a}, \\ K_{1A_2} &= K_{1B_1} = F_{1B_1}(2a/d)p\sqrt{\pi a}. \end{aligned} \tag{15}$$

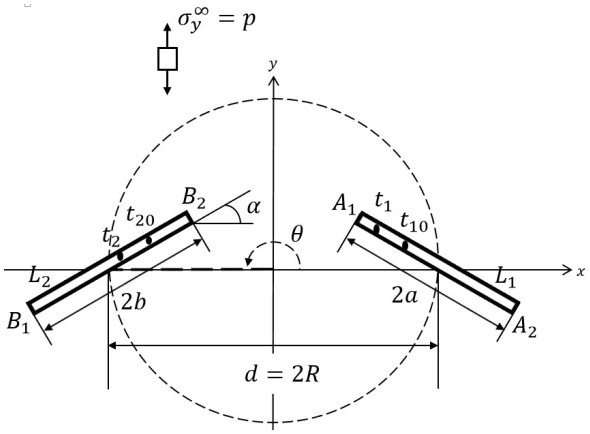

Fig. 2 Two equal inclined cracks in an infinite plate.

Table 1 shows the calculated values of F_{1B_1} and F_{1B_2}. It exhibits that our results have a good agreement with those of [6].

Table 1 A comparison of the nondimensional SIFs for two inclined cracks in an infinite plate with the previous numerical computation.

	$\alpha = 20°$				$\alpha = 30°$			
$2a/d$	${F_{1B_1}}^*$	${F_{1B_1}}^{**}$	${F_{1B_2}}^*$	${F_{1B_2}}^{**}$	${F_{1B_1}}^*$	${F_{1B_1}}^{**}$	${F_{1B_2}}^*$	${F_{1B_2}}^{**}$
0.1	0.8839	0.8847	0.8839	0.8847	0.7513	0.7503	0.7502	0.7503
0.2	0.8861	0.8866	0.8870	0.8877	0.7514	0.7516	0.7520	0.7522
0.3	0.8898	0.8900	0.8927	0.8934	0.7537	0.7534	0.7560	0.7559
0.4	0.8950	0.8956	0.9021	0.9027	0.7559	0.7560	0.7620	0.7620
0.5	0.9016	0.9023	0.9169	0.9175	0.7596	0.7595	0.7718	0.7718
0.6	0.9102	0.9108	0.9398	0.9404	0.7642	0.7640	0.7872	0.7871
0.7	0.9213	0.9218	0.9763	0.9767	0.7701	0.7698	0.8110	0.8110
0.8	0.9359	0.9363	1.0381	1.0382	0.7777	0.7775	0.8492	0.8490
0.9	0.9570	0.9570	1.1590	1.1600	0.7886	0.7881	0.9140	0.9140

* Present method

** Denda and Dong [6]

Figures 3 and 4 plot the nondimensional SIF against the angle of positions of second crack, θ, for two inclined cracks with the angle of inclination is $\alpha_1 = \alpha_2 = 20°$ and $60°$, respectively, (Fig. 1). The calculated SIFs at the crack tips A_1, A_2, B_1, and B_2 are defined as

$$\begin{aligned} K_{iA_j} &= F_{iA_j}(\theta, b/a)p\sqrt{\pi a}, \\ K_{iB_j} &= F_{iB_j}(\theta, b/a)p\sqrt{\pi a}, \quad i, j = 1, 2. \end{aligned} \tag{16}$$

In Fig. 3, for the case $b/a = 0.1$, since the second crack is much smaller than the first crack, the nondimensional SIFs at the first crack tips (Figs. 3a and 3b) are not fluctuating significantly, while the nondimensional SIFs at the second crack tips (Figs. 3c and 3d) are varying significantly. The shielding effect on the second crack tips (Figs. 3c and 3d) for $b/a = 0.5$ and 1.0 is found to be more stronger than the first crack tips (Figs. 3a and 3b) with an increasing angle θ. The finding shows that the severity on the second crack is obvious as its length is half or equal to the first crack length.

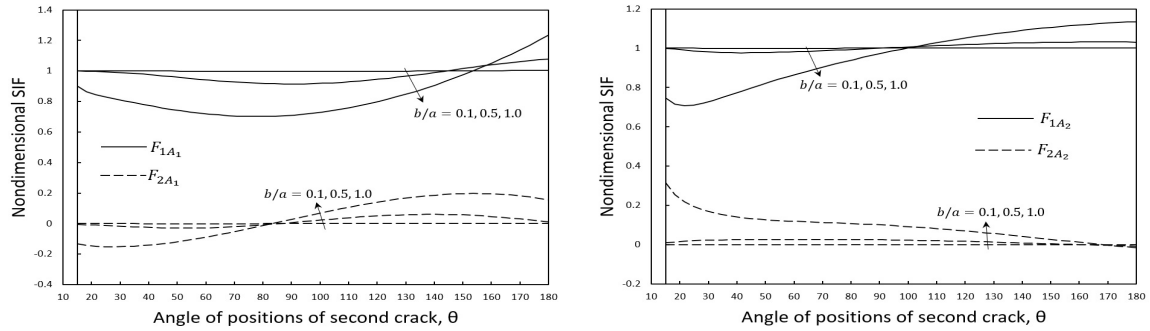

(a) Nondimensional SIF at the crack tip A_1

(b) Nondimensional SIF at the crack tip A_2

(c) Nondimensional SIF at the crack tip B_1

(d) Nondimensional SIF at the crack tip B_2

Fig. 3 Nondimensional SIF for two inclined cracks with $\alpha_1 = \alpha_2 = 20^\circ$ when θ is changing.

Figure 4 shows that the shielding effect on the second crack tips (Figs. 4c and 4d) is more significant than the first crack tips (Figs. 4a and 4b). These observations show that the second crack is most affected as the angle θ increased. In addition, the severity on the second crack for $\alpha_1 = \alpha_2 = 60^\circ$ (Fig. 4) is more serious than $\alpha_1 = \alpha_2 = 20^\circ$ (Fig. 3). For example, in the case of $b/a = 0.1$ and $\theta = 48^\circ$, the results for $\alpha_1 = \alpha_2 = 60^\circ$ are $F_{1B_1} = 0.38690$ and $F_{1B_2} = 0.49104$, while for $\alpha_1 = \alpha_2 = 20^\circ$, we have $F_{1B_1} = 0.32533$ and $F_{1B_2} = 0.31436$.

Figure 5 represents the nondimensional SIF versus the ratio b/a for $\alpha_1 = \alpha_2 = 20^\circ$. It can be seen that the crack tips has the highest value of F_1 at the angle $\theta = 180^\circ$ than at the angle $\theta = 15^\circ$ and 90°. That is to say, both cracks have more shielding effect at the angle $\theta = 180^\circ$. In addition, at an angle $\theta = 15^\circ$, the values of F_{1A_1} and F_{1A_2} decreased whereas the values of F_{1B_1} and F_{1B_2} increased as the ratio b/a increased. These observations show that at an angle $\theta = 15^\circ$, as the length of the second crack increases, the severity at the second crack tips is more significant than the first.

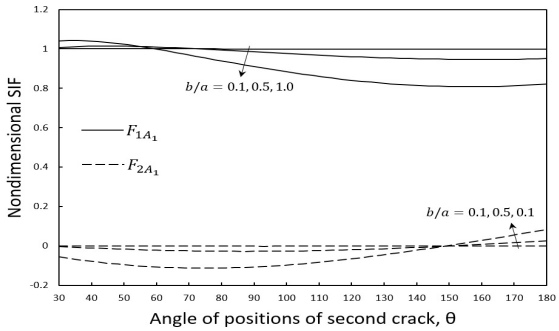

(a) Nondimensional SIF at the crack tip A_1

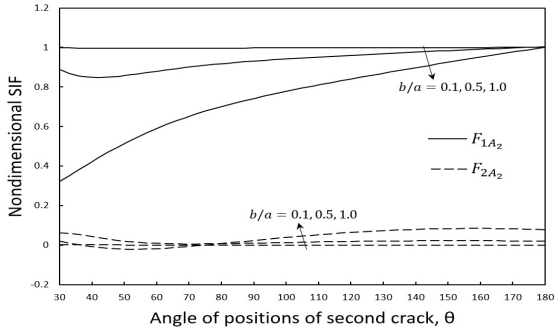

(b) Nondimensional SIF at the crack tip A_2

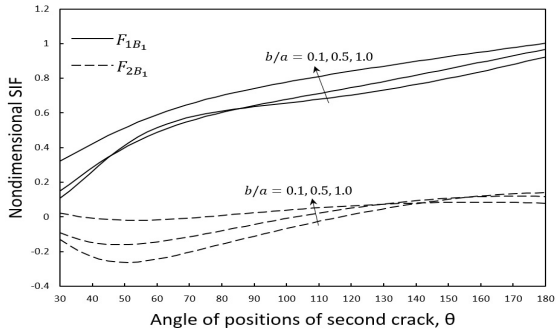

(c) Nondimensional SIF at the crack tip B_1

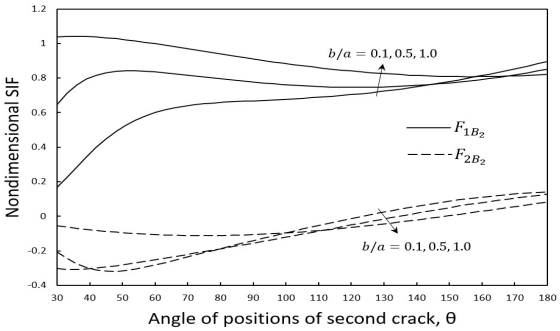

(d) Nondimensional SIF at the crack tip B_2

Fig. 4 Nondimensional SIF for two inclined cracks with $\alpha_1 = \alpha_2 = 60^\circ$ when θ is changing.

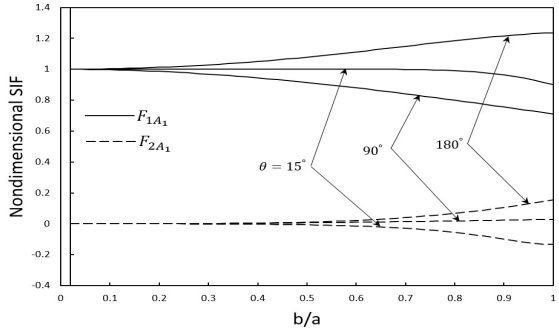

(a) Nondimensional SIF at the crack tip A_1

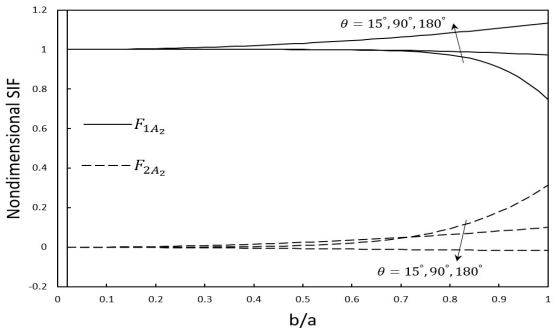

(b) Nondimensional SIF at the crack tip A_2

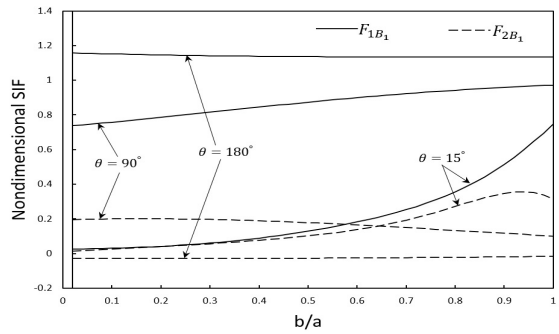

(c) Nondimensional SIF at the crack tip B_1

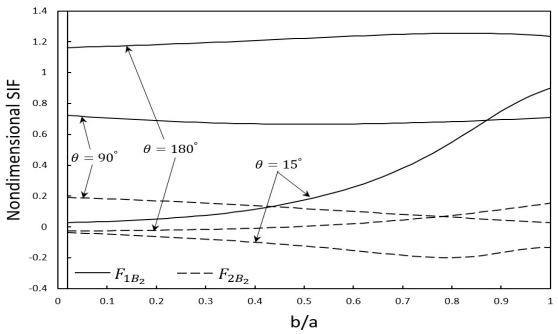

(d) Nondimensional SIF at the crack tip B_2

Fig. 5 Nondimensional SIF for two inclined cracks when $\alpha_1 = \alpha_2 = 20^\circ$ as b/a changing.

4.2 Example 2

Consider two curved cracks subjected to the remote tension $\sigma_x^\infty = \sigma_y^\infty = p$ (Figs. 6 and 7). The radius of L_1 and L_2 is denoted as R_1 and R_2, respectively. The calculated results for the SIFs at crack tips A_1, A_2, B_1, and B_2 are

$$\begin{aligned} K_{iA_j} &= F_{iA_j}(\theta, R_2/R_1)p\sqrt{\pi a}, \\ K_{iB_j} &= F_{iB_j}(\theta, R_2/R_1)p\sqrt{\pi a}, \qquad i,j = 1,2. \end{aligned} \tag{17}$$

The obtained results for the problems in Fig. 6 for $R_1/R = 0.9$ and $\theta = 180^\circ$ are listed in Table 2.

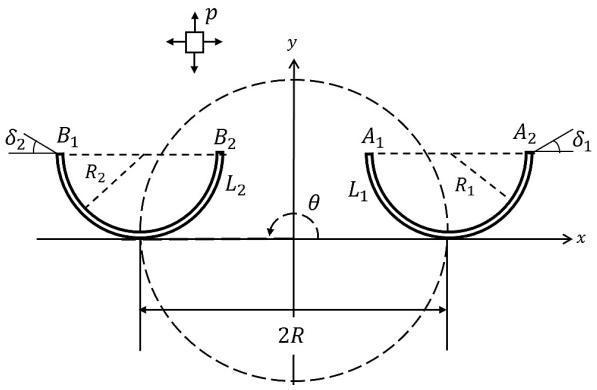

Fig. 6 Two curved cracks in an infinite plate.

Table 2 Nondimensional SIFs for the problem shown in Fig. 6.

R_2/R_1	F_{1A_1}	F_{2A_1}	F_{1A_2}	F_{2A_2}	F_{1B_1}	F_{2B_1}	F_{1B_2}	F_{2B_2}
0.1	0.3753	-0.3776	0.3764	0.3775	0.3030	-0.4386	0.3286	0.4598
0.2	0.3725	-0.3797	0.3764	0.3788	0.3165	-0.4415	0.3166	0.4663
0.3	0.3685	-0.3840	0.3763	0.3809	0.3294	-0.4425	0.3039	0.4729
0.4	0.3643	-0.3912	0.3763	0.3840	0.3416	-0.4421	0.2908	0.4798
0.5	0.3605	-0.4017	0.3764	0.3882	0.3529	-0.4410	0.2772	0.4863
0.6	0.3582	-0.4163	0.3770	0.3936	0.3632	-0.4388	0.2642	0.4923
0.7	0.3580	-0.4358	0.3785	0.4003	0.3726	-0.4365	0.2539	0.4978
0.8	0.3607	-0.4614	0.3814	0.4086	0.3812	-0.4345	0.2511	0.5027
0.9	0.3631	-0.4937	0.3866	0.4189	0.3888	-0.4327	0.2678	0.5084
1.0	0.3297	-0.5316	0.3949	0.4324	0.3949	-0.4324	0.3297	0.5316

For the problem in Fig. 7, the results are plotted in Figs. 8 and 9. Figure 8 presents the nondimensional SIF versus the angle of positions of second crack, θ. Figure 8a shows that the values of F_1 for the crack tip A_1 when $R_2/R_1 = 0.1$, 0.5, 0.9 have the maximum value at the angle $\theta = 82^\circ, 79^\circ$ and 79°, respectively. This result can be explained by observing that at each angle θ, the crack tip A_1 lies very closed to the second crack. In Fig. 8b, there is a significant effect at $R_2/R_1 = 0.9$ as the angle θ increased. Figure 8c exhibits that the severity at the crack tip B_1 is significant at the angle $\theta = 79^\circ$ for the case $R_2/R_1 = 0.9$. From the data in Fig. 8d, it is apparent that the nondimensional SIFs fluctuate as the angle θ increased. This result has shown that the second crack has a strong shielding effect on the crack tip B_2.

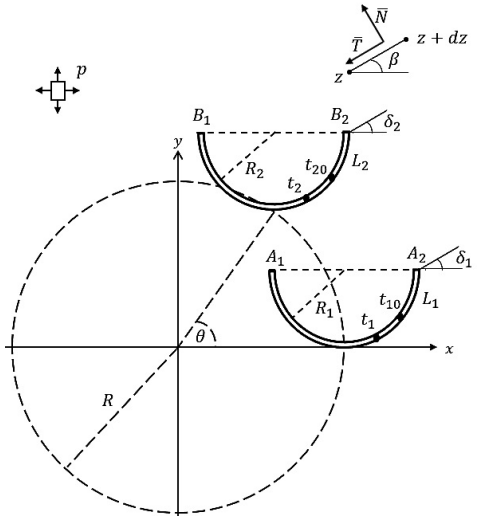

Fig. 7 Two curved cracks placed in a circular position in plane elasticity.

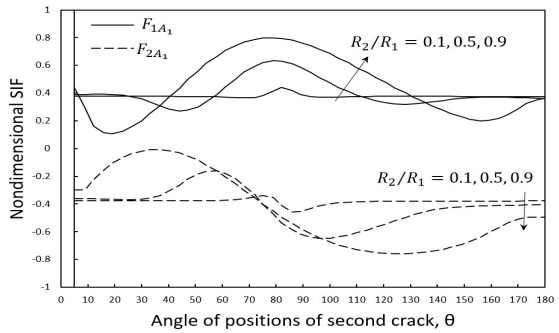

(a) Nondimensional SIF at the crack tip A_1

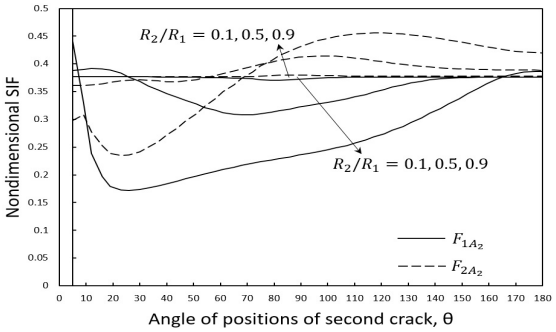

(b) Nondimensional SIF at the crack tip A_2

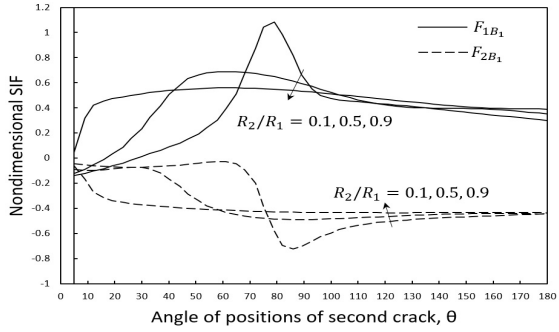

(c) Nondimensional SIF at the crack tip B_1

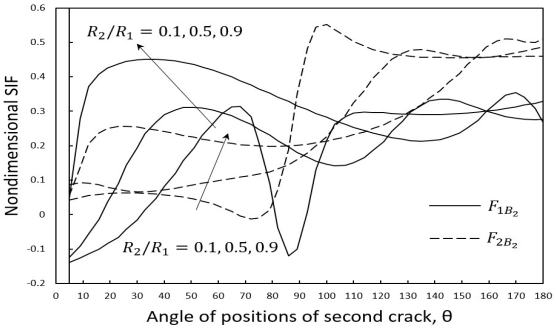

(d) Nondimensional SIF at the crack tip B_2

Fig. 8 Nondimensional SIF for two curved cracks as θ varies.

Figure 9 shows the graphs of nondimensional SIF versus the ratio R_2/R_1. For $\theta = 180°$, there has been a slight change of the nondimensional SIF values at the first (9a and 9b) and second cracks tips (9c and 9d) as the ratio R_2/R_1 increased. This observation shows that at an angle $\theta = 180°$, the severity at both curved cracks tips is not significant. In Figs. 9a and 9b, the effect at $\theta = 90°$ on the value of F_1 is higher than $\theta = 55°$. From Fig. 9c, as $R_2/R_1 \geq 0.34$, the effect at $\theta = 55°$ on the value of F_1 is higher than $\theta = 90°$, and in Fig. 9d, the effect at $\theta = 55°$ on the value of F_1 is higher than $\theta = 90°$ as R_2/R_1 increased.

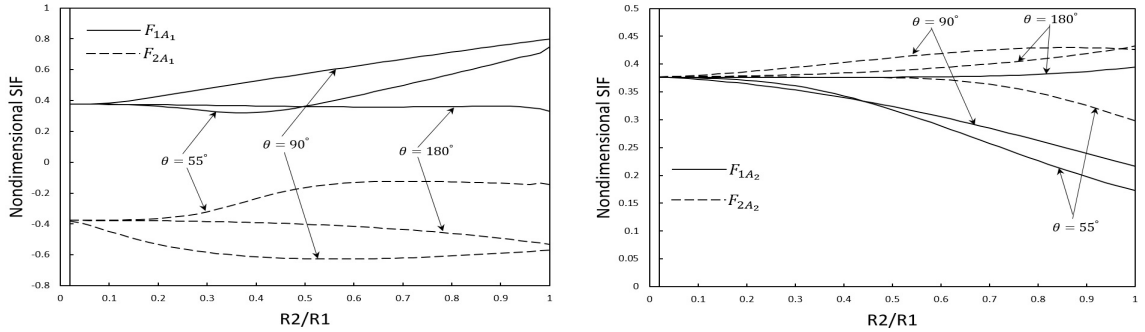

(a) Nondimensional SIF at the crack tip A_1

(b) Nondimensional SIF at the crack tip A_2

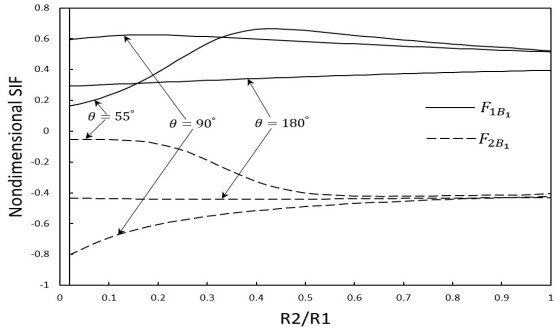

(c) Nondimensional SIF at the crack tip B_1

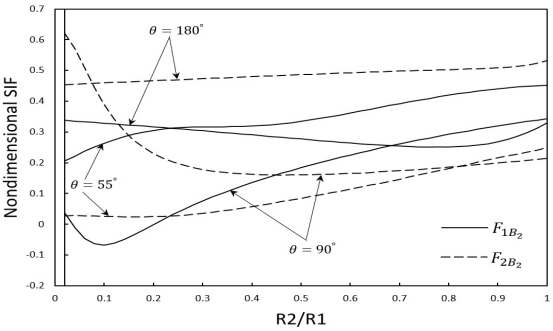

(d) Nondimensional SIF at the crack tip B_2

Fig. 9 Nondimensional SIF for two curved cracks when R_2/R_1 changing.

4.3 Example 3

Consider the interaction between curved and inclined cracks in circular positions (Fig. 10). The remote tension is $\sigma_x^\infty = \sigma_y^\infty = p$. The calculated results for the SIFs at the crack tips A_1, A_2, B_1, and B_2 are

$$\begin{aligned} K_{iA_j} &= F_{iA_j}(\theta) p\sqrt{\pi a}, \\ K_{iB_j} &= F_{iB_j}(\theta) p\sqrt{\pi a}, \qquad i,j = 1,2. \end{aligned} \tag{18}$$

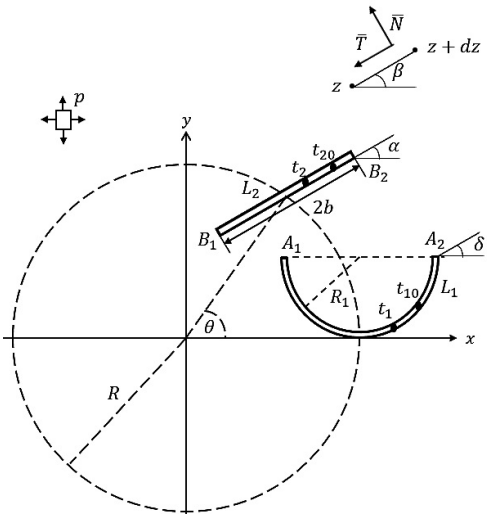

Fig. 10 Curved and inclined cracks placed in a circular position in plane elasticity.

Figure 11 demonstrates the nondimensional SIF versus the angle of positions of second crack, θ, for $\alpha = 20°$. Figure 11a presents the nondimensional SIFs for $b/R_1 = 0.1$ and $\delta = 85°$ at the angle $6° \leq \theta \leq 180°$. The result shows that the shielding effect on the crack tips of inclined crack (B_1 and B_2) is most obvious at $40° < \theta < 120°$, but then less significant effect on the curved crack tips (A_1 and A_2) as θ increased. The highest value of F_{1B_1} is found at the angle $\theta = 90°$ with the value $F_{1B_1} = 1.46010$, while for F_{1B_2} the same phenomenon happen at $\theta = 99°$ with the value $F_{1B_2} = 1.42263$. Figure 11b exhibits the nondimensional SIFs for the ratio $b/R_1 = 0.5$ and $\delta = 45°$ at the angle $30° \leq \theta \leq 180°$. As $\theta < 130°$, the shielding effect on the inclined crack is significant. Meanwhile, the effect on the curved crack is more obvious on the crack tip A_1 than A_2 as θ increased. Figures 11c and 11d show the nondimensional SIFs for the ratio of $b/R_1 = 0.9$ and 1.0, respectively, when $\delta = 45°$ at the angle $36° \leq \theta \leq 180°$. Since the angle θ is varied, the shielding effect on the curved and inclined cracks is easily seen. However, the value of SIF at the right crack tip of inclined crack (B_1) is not significant as the angle θ increased.

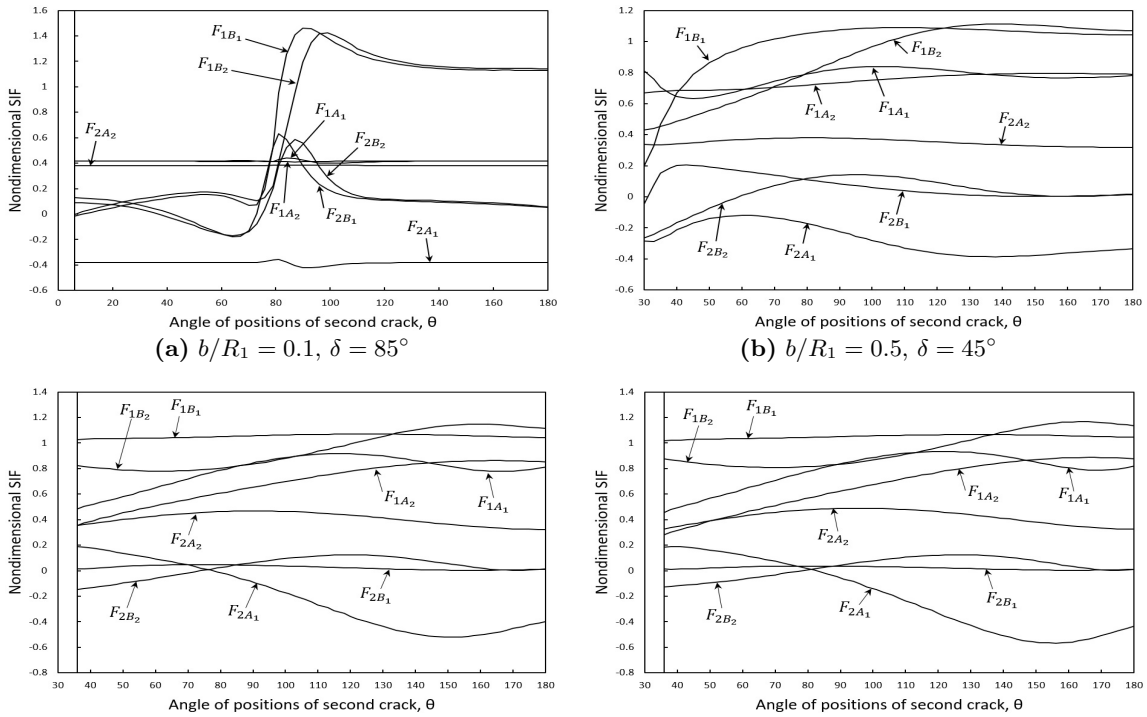

(a) $b/R_1 = 0.1$, $\delta = 85°$ **(b)** $b/R_1 = 0.5$, $\delta = 45°$

(c) $b/R_1 = 0.9$, $\delta = 45°$ **(d)** $b/R_1 = 1.0$, $\delta = 45°$

Fig. 11 Nondimensional SIF for $\alpha = 20°$ when θ changing.

Figure 12 illustrates the nondimensional SIF against the ratio b/R_1 for $\alpha = 30°$ where the SIF at the crack tips are defined as

$$\begin{aligned} K_{iA_j} &= F_{iA_j}(b/R_1)p\sqrt{\pi a}, \\ K_{iB_j} &= F_{iB_j}(b/R_1)p\sqrt{\pi a}, \quad i,j = 1,2. \end{aligned} \tag{19}$$

Figures 12a and 12b have a similar pattern of nondimensional SIF. They show that the values of F_{1A_1} and F_{1A_2} are gradually decreased, while the values of F_{1B_1} and F_{1B_2} are gradually increased. These observations show that, as the ratio b/R_1 increased, the severity at the inclined crack tips is significant compared to the effect on the curved crack tips. In Fig. 12c, it is found that the values of F_{1B_1} and F_{1B_2} take rather higher value than the values of F_{1A_1} and F_{1A_2}. In addition, the inclined crack tips are more severe at $b/R_1 = 0.02$. Figure 12d depicts the severity on the cracks tips at the angle $\theta = 180°$ is not significant as the ratio b/R_1 increased.

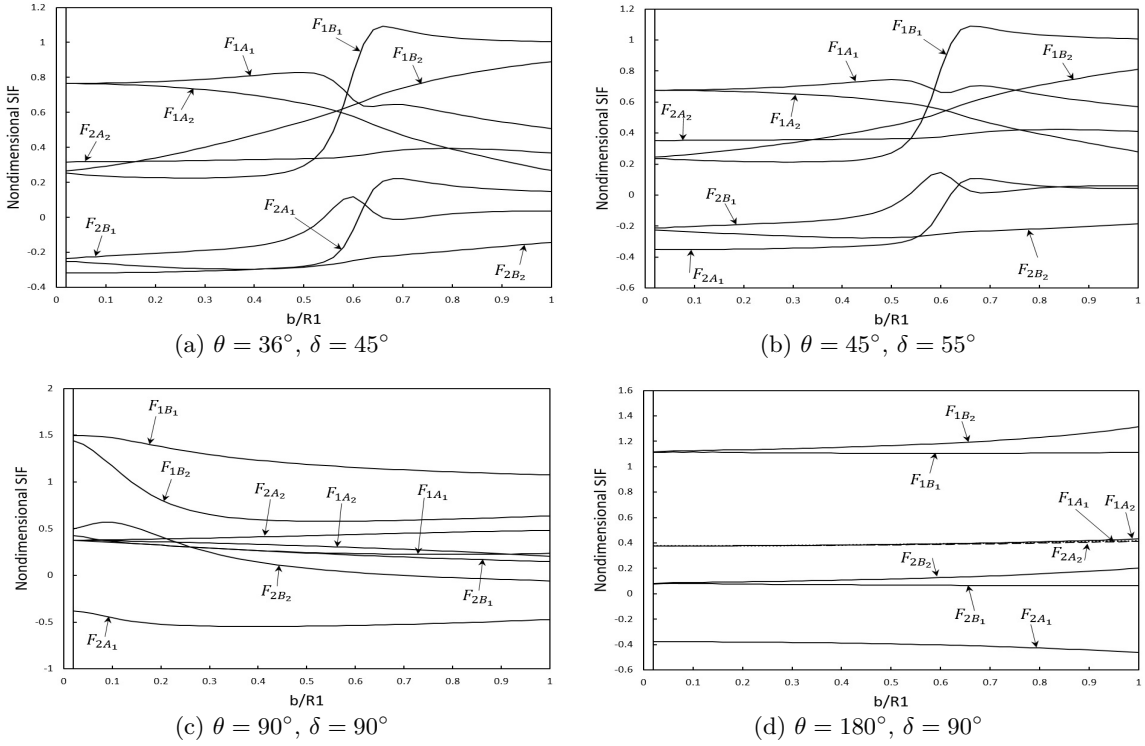

(a) $\theta = 36^\circ$, $\delta = 45^\circ$ (b) $\theta = 45^\circ$, $\delta = 55^\circ$

(c) $\theta = 90^\circ$, $\delta = 90^\circ$ (d) $\theta = 180^\circ$, $\delta = 90^\circ$

Fig. 12 Nondimensional SIF for $\alpha = 30^\circ$ when b/R_1 changing.

5 Conclusion

The multiple cracks problems in a circular position in plane elasticity are studied. The hypersingular integral equation for two cracks have been formulated. The numerical examples showed the behaviour of the stress state at the crack tips. Since the angle θ is varied, it is obvious that the second crack tips is most affected than that at the first crack tips. In addition, with an increase of the length ratio of the second to the first crack, the shielding effect for the cracks at the angle $\theta \leq 90^\circ$ is obvious.

Acknowledgements The second author would like to thank Universiti Putra Malaysia (UPM), Malaysia for the Putra Grant, Vot No. 9442300.

References

1. Muskhelishvili, N.I.: Some basic problems of the mathematical theory of elasticity. Noordhoff International Publishing, Leyden (1953)
2. Chen, Y.Z., Hasebe, N., Lee, K.Y.: Multiple crack problems in elasticity. WIT press, Southampton (2003)
3. Nik Long, N.M.A., Eshkuvatov, Z.K.: Hypersingular integral equation for multiple curved cracks problem in plane elasticity. Int. J. Solids Struct. **46**, 2611–2617 (2009)
4. Mayrhofer, K., Fisher, D.: Derivation of a new analytical solution for a general two dimensional finite-part integral applicable in fracture mechanics. Int. J. Numer. Meth. Eng. **33**, 1027–1047 (1992)
5. Nik Long, N.M.A., Aridi, M.R., Eshkuvatov, Z.K.: Mode stresses for the interaction between an inclined crack and a curved crack in plane elasticity. Math. Probl. Eng. (2015)
6. Denda, M., Dong, Y.F.: Complex variable approach to the BEM for multiple crack problems. Comput. Methods Appl. Mech. Eng. **141**, 247–264 (1997)
7. Vialaton, G., Lhermet, G., Vessiere, G., Boivin, M., Bahuaud, J.: Field of stresses in an infinite plate containing two collinear cuts loaded at an arbitrary location. Eng. Fract. Mech. **8**, 525–538 (1976)
8. Panasyuk, V.V., Savruk, M.P., Datsyshyn, A.P.: A general method of solution of two-dimensional problems in the theory of cracks. Eng. Fract. Mech. **9**, 481–497 (1977)
9. Kachanov, M.: A simple technique of stress analysis in elastic solids with many cracks. Int. J. Fract. **28**, R11–R19 (1985)
10. Kachanov, M.: Elastic solids with many cracks: A simple method of analysis. Int. J. Solids Struct. **23**(1), 23–43 (1987)

11. Chen, Y.Z.: Singular integral equation method for the solution of multiple curved crack problems. Int. J. Solids Struct. **41**, 3505–3519 (2004)
12. Chen, Y.Z., Lin, X.Y.: Numerical solution of singular integral equation for multiple curved branch-cracks. Struct. Eng. Mech. **34**, 85–95 (2010)
13. Helsing, J.: A fast and stable solver for singular integral equations on piecewise smooth curved. SIAM J. Sci. Comput. **33**, 153–174 (2011)
14. Chen, Y.Z.: General case of multiple crack problems in an infinite plate. Eng. Fract. Mech. **20**, 591–597 (1984)
15. Chen, Y.Z.: New Fredholm integral equation for multiple crack problem in plane elasticity and antiplane elasticity. Int. J. Fract. **64**, 63–77 (1993)
16. Chen, Y.Z.: A survey of new integral equations in plane elasticity crack problem. Eng. Fract. Mech. **51**, 97–134 (1995)
17. Chen, Y.Z.: Hypersingular integral equation approach for the multiple crack problem in an infinite plate. Acta Mech. **108**, 121–131 (1995)
18. Chen, Y.Z.: A numerical solution technique of hypersingular integral equation for curved cracks. Commun. Numer. Meth. Eng. **19**, 645–655 (2003)
19. Aridi, M.R., Nik Long, N.M.A., Eshkuvatov, Z.K.: Mode stresses for the interaction between straight and curved cracks problem in plane elasticity. J. Appl. Math. Phys. **2**, 225–234 (2014)
20. Zozulya, V.V.: Regularization of hypersingular integrals in 3-D fracture mechanics: Triangular BE, and piecewise-constant and piecewise-linear approximations. Eng. Anal. Bound. Elem. **34**, 105–113 (2010)
21. Wang, X., Ang, W.T., Fan, H.: Hypersingular integral and integro-differential micromechanical models for an imperfect interface between a thin orthotropic layer and an orthotropic half-space under inplane elastostatic deformations. Eng. Anal. Bound. Elem. **52**, 32–43 (2015)